Journal of The Electrochemical Society, **158** (12) K213-K216 (2011)
0013-4651/2011/158(12)/K213/4/$28.00 © The Electrochemical Society

Graphene-Based Antidots for Thermoelectric Applications

Hossein Karamitaheri,[a,d,z] Mahdi Pourfath,[b,d] Meysam Pazoki,[c] Rahim Faez,[a] and Hans Kosina[d]

[a]*School of Electrical Engineering and* [c]*Department of Physics, Sharif University of Technology, Tehran, Iran*
[b]*Electrical and Computer Engineering Deparment, University of Tehran, Tehran, Iran*
[d]*Institute for Microelectronics, Technische Universität Wien, A-1040 Wien, Austria*

The low temperature thermoelectric properties of hydrogen-passivated graphene-based antidot lattices are theoretically investigated. Calculations are performed using density functional theory in conjunction with the Landauer formula to obtain the ballistic transport coefficients. Antidot lattices with hexagonal, triangular and rectangular antidot shapes are studied. Methods to reduce the thermal conductance and to increase the thermoelectric power factor of such structures are studied. Our results indicate that triangular antidot lattices have the smallest thermal conductance due to longer boundaries, the smallest distance between the neighboring antidots, and the armchair edges. This structure has the largest electronic band-gap and its figure of merit is the highest among other antidots in a wide range of temperature.
 [DOI: 10.1149/2.025112jes]

Manuscript submitted July 12, 2011; revised manuscript received August 11, 2011. Published October 31, 2011. This was Paper 1206 presented at the Montreal, QC, Canada, Meeting of the Society, May 1–6, 2011.

Today, thermoelectric devices are used in a very wide range of applications including energy harvesting, aerospace, and military applications. The thermoelectric figure of merit is defined as:

$$ZT = \frac{S^2 GT}{(K_{\text{el}} + K_{\text{ph}})} \quad [1]$$

where S denotes the Seebeck coefficient, G the electrical conductance, T the temperature, K_{el} the electrical and K_{ph} the lattice contributions to the thermal conductance. The numerator of Z is called power factor. The figure of merit determines the efficiency of a thermoelectric device and can be improved by increasing the power factor and decreasing the thermal conductance. Hence, good thermoelectric materials should simultaneously have a high Seebeck coefficient, a high electrical conductance, and a low thermal conductance.

While each property of ZT can individually be changed by several orders of magnitude, the interdependence and coupling between these properties have made it extremely difficult to increase ZT to values greater than one. Bismuth and its alloys that are commonly used in thermoelectric applications[1] suffer from high cost. On the contrary, bulk silicon has a very low $ZT \approx 0.01$ because of its high thermal conductance.[2]

In recent years many studies have been conducted on employing new materials and technologies to improve ZT. Progress in synthesis of nanomaterials has allowed the realization of low-dimensional thermoelectric device structures such as one-dimensional nanowires, thin films, and two-dimensional superlattices.[3–5] However, the recent breakthroughs in materials with $ZT > 1$ have mainly benefited from reduced phonon thermal conductance.[5,6]

Graphene, a recently discovered form of carbon, has received much attention over the past few years due to its excellent electrical, optical, and thermal properties.[7] The electrical conductance of graphene is as high as that of copper[8] and a large Seebeck coefficient has been predicted in a graphene-based nanostructure.[9] In addition, a large scale method to produce graphene sheets has been reported.[10] These factors render graphene as a candidate for future thermoelectric applications.

However, the ability of graphene to conduct heat is an order of magnitude higher than that of copper.[11] Therefore, it is necessary to reduce its thermal conductance. The high thermal conductance of graphene is mostly due to the lattice contribution, whereas the electronic contribution to the thermal conduction can be ignored.[11,12] Therefore, by proper engineering of phonon transport properties it is possible to reduce the total thermal conductance without significant reduction of the electrical conductance and the power factor. Recently many theoretical studies have been performed on the thermal conductivity of graphene-based structures. It has been shown that boundaries and edge roughness can strongly influence the thermal conductance.[13,14] Vacancy, defects, hydrogen passivation, and isotope doping can have significant effects on thermal conductance.[14–16]

Graphene Antidot Lattices

In this work we investigate the thermoelectric properties of a new graphene-based structure called graphene antidot lattice (GAL).[17] Since a realistic structure contains hydrogen terminated edges, all the suspended bonds at the edges of the antidots are passivated with hydrogen atoms using a carbon-hydrogen bond length of 1.1 Å. The electrical and optical properties of GALs with high symmetry hexagonal and triangular antidots have been theoretically studied in Refs. 18, 19, and 20 The results indicate that by introducing regular patterns of antidots in a graphene sheet, it is possible to achieve a direct band-gap semiconductor from a semi-metal pristine graphene sheet. Although this issue plays an important role in thermoelectric applications, the Seebeck coefficient is sensitive to the details of the electronic band structure and the asymmetry between electrons and holes.[21,22] In this paper we investigate the effect of the geometrical parameters of antidots on the thermoelectric properties of hydrogen-passivated (H-passivated) GALs in a temperature range of 10 K to 300 K. We study GALs with hexagonal, triangular, and rectangular antidot shapes. We show that by introducing antidots in the graphene sheet (Fig. 1) the thermal conductances of GALs decrease and thus the respective ZT values are increased.

The unit cell of a H-passivated GAL can be described by three parameters L, N_C, and N_H, where L is the side length of the hexagon in terms of the graphene lattice constant ($a = 2.46$ Å), N_C is the number of carbon atoms that are removed from the pristine supercell, and N_H is the number of hydrogen atoms which is equal to the number of edge carbon atoms. We consider antidots of hexagonal (Hex), isotriangular (IsoTri), and rectangular (Rect) shape as shown in Fig. 1. Fig. 1-a shows a hexagonal antidot which is formed by removing 96 carbon atoms from a cell with $L = 8$. It has 24 edge atoms, therefore, it is represented by Hex(8, 96, 24).

Approach

We employed the ab-initio simulation package SIESTA[23] to study the electronic and phononic band structure of H-passivated GALs. We use a double zeta polarized basis set with a mesh cut-off of 125 Ry. The general gradient approximation for the exchange correlation potential is used with a functional proposed by Perdew et al.[24] Brillouin zone sampling was carried out by a $10 \times 10 \times 1$ Monkhorst-Pack grid.

[z] E-mail: karami@iue.tuwien.ac.at

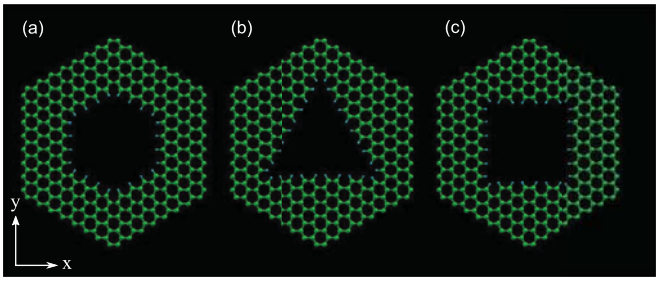

Figure 1. Geometrical structures of different GALs. (a)–(c) indicate Hex(8, 96, 24), IsoTri(8, 90, 30), and Rect(8, 104, 24), respectively. Hydrogen atoms are shown in blue color. Transport is assumed to be along the x-direction.

For structural relaxations, the positions of the atoms are changed until the force acting on each atom becomes smaller than 0.03 eV/Å. Self-consistency in the total energy is achieved with a tolerance of less than 10^{-4} Ry. For phonon calculations, the force constant matrix is calculated by displacing each atom 0.04 Bohr along the coordinate directions around its equilibrium position and evaluating the forces exerted from the other atoms.

After obtaining the band structures of electrons and phonons, we evaluate the ballistic transmission probability $\overline{T}(E)$ for both electrons and phonons:[25–27]

$$\overline{T}(E)|_{\text{Ballistic}} = M(E) = \sum_{k_\perp} \Theta[E - \varepsilon(k_\perp)] \qquad [2]$$

where $M(E)$ denotes the density of modes, Θ is the unit step function, and $k_\perp$ refers to the wave vector component perpendicular to the transport direction.[28] Within the framework of the Landauer theory,[29] in the linear response regime one can express the electrical conductance, Seebeck coefficient, and electronic thermal conductance as:

$$G = \left(\frac{2q^2}{h}\right) I_0 \quad [1/\Omega] \qquad [3]$$

$$S = \left(-\frac{k_B}{q}\right) \frac{I_1}{I_0} \quad [V/K] \qquad [4]$$

$$K_{el} = \left(\frac{2Tk_B^2}{h}\right) \left[I_2 - \frac{I_1^2}{I_0}\right] \quad [W/K] \qquad [5]$$

respectively.[28] Here, h is the Planck constant, $f(E)$ is the Fermi function, $\overline{T}_{el}(E)$ is the electronic transmission probability and

$$I_j = \int_{-\infty}^{+\infty} \left(\frac{E - E_F}{k_B T}\right)^j \overline{T}_{el}(E) \left(-\frac{\partial f}{\partial E}\right) dE \qquad [6]$$

where k_B is the Boltzmann constant and E_F is the Fermi-level of the system. The derivative of the Fermi function is known as the thermal broadening which has a width of a few $k_B T$ around E_F. The lattice contribution to the thermal conductance can be given as a function of the phonon transmission probability:[15]

$$K_{ph} = \frac{1}{h} \int_0^{+\infty} \overline{T}_{ph}(\omega) \hbar\omega \left(\frac{\partial n(\omega)}{\partial T}\right) d(\hbar\omega) \qquad [7]$$

where $n(\omega)$ denotes the Bose-Einstein distribution function and $\overline{T}_{ph}(\omega)$ is the phonon transmission probability.

The Role of Geometrical Parameters

The electron transmission probabilities of three GALs along the x-coordinate are shown in Fig. 2. In pristine graphene there is a global balance between the number of carbon atoms in each sublattice. Here, this global balance is not disturbed by introducing the antidots. Beside this global balance, there is also a local sublattice balance

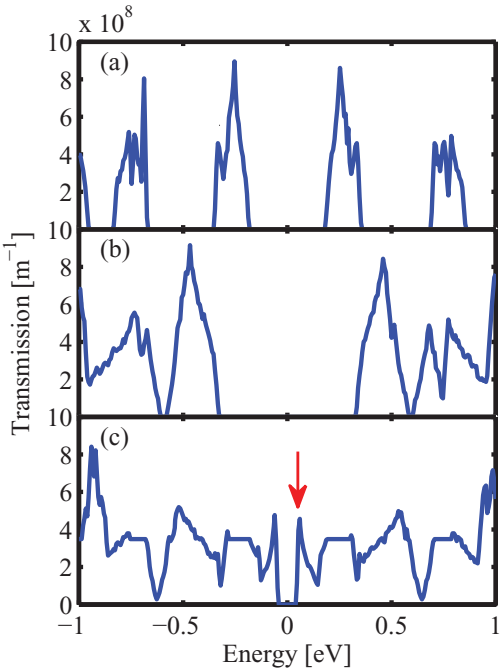

Figure 2. The electron transmission probability of (a) Hex(8, 96, 24), (b) IsoTri(8, 90, 30), and (c) Rect(8, 104, 28).

in GALs. Therefore, they have not any flat or quasi-flat band near the Fermi level.[30,31] By introducing antidots in the graphene sheet, the zero band-gap graphene can be converted into a narrow band-gap semiconductor[20,32] (see Fig. 2). As a zero band-gap material, pristine graphene has a very small Seebeck coefficient,[33] whereas GALs have a beneficial band-gap, so that one can suppress either the electron or the hole current to obtain unipolar conduction.

In the hexagonal GAL, the band-gap is nearly 0.35 eV and the width of the first conduction subband is 0.15 eV. The band-gap of the rectangular GAL is very small. However, it has a sharp edge in transmission probability near the first conduction subband edge (see the arrow in Fig. 2-c). The first conduction subband of IsoTri(8,90,30) shows a band-gap of nearly 0.65 eV and a width of 0.25 eV. While there is an energy gap between the first and second conduction subband in Hex(8,96,24), these two subbands contact each other in Iso(8,90,30).

It has been proposed that sharp features in the density of states along with a proper band-gap will enhance the Seebeck coefficient[34] and that the sharp features in the transmission probabilities of GALs will have an important effect on the thermoelectric properties of a nanoscale device. In the following, we study the thermoelectric properties of GALs and present the role of temperature.

At room temperature, the factor $\partial f/\partial E$ has significant values only in the range of 0.2 eV around the Fermi level. Under the condition $E_G > 0.2$ eV, the hole contribution to the total electrical current will be suppressed. As a result, a large value of the Seebeck coefficient is obtained. Fig. 3-a shows the Seebeck coefficient of GALs with different antidot shapes versus the Fermi level. The peak of the Seebeck coefficient of IsoTri(8,90,30) is the highest compared with other GALs, because of its large electronic band-gap. The power factor of GALs is maximum for the Fermi level equal to the conduction band edge. The peak of the power factor of Hex(8,96,24) is larger than that of IsoTri(8,90,30), because of a sharp feature in the transmission probability of Hex(8,96,24) (see Fig. 3-c) which results in a 18% increase in electrical conductance of Hex(8,96,24) with respect to that of IsoTri(8,90,30). Therefore, hexagonal GALs can have the highest power factor.

By introducing antidots into the graphene sheet, some phonon modes become less dispersive, similar to electrons, and their contribution to the thermal conductance becomes negligible. Beside the

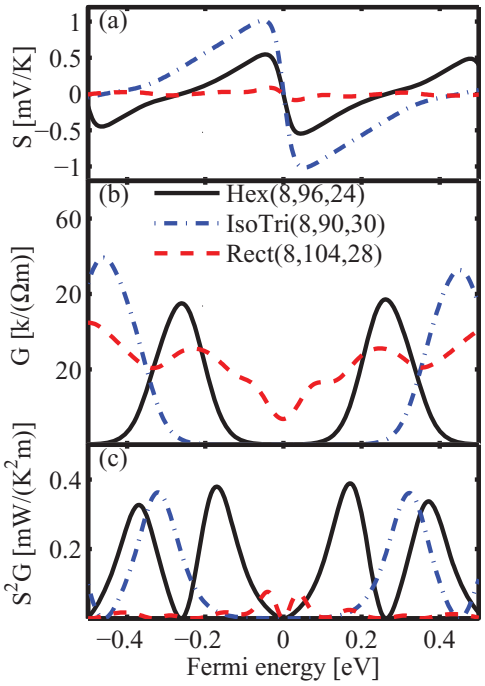

Figure 3. (a) The Seebeck coefficient, (b) the electrical conductance, and (c) the power factor of GALs as a function of the Fermi energy.

size of the antidot, the number of edge atoms and the distance between neighboring antidots have an important effect on the transmission probabilities. Furthermore, it has been recently shown that hydrogen-passivation of GNR edges has different effects on the thermal conductance of GNRs with different chiralities.[14] To investigate the effect of these parameters, we compare the thermal conductance of GALs with nearly the same area and different shapes, including Hex(8,96,24), IsoTri(8,90,30), and Rect(8,104,28). Although the DOS of these GALs are in the same order, their transmission probabilities can be very different.

As shown in Fig. 4, Hex(8,96,24) has the highest and IsoTri(8,90,30) the lowest transmission probabilities, especially at low frequencies. The lattice thermal conductivity is dominated by low frequency phonons. Therefore, one can expect the thermal conductance of these GALs to be quite different. Although the area of IsoTri(8,90,30) is smaller than that of Hex(8,96,30), its thermal conductance is nearly 20% smaller. This can be explained by the 25% larger circumference and a smaller distance between the nearest

Table I. Comparison of the thermal conductances of different GALs. The results are normalized to the thermal conductance of pristine graphene.

	Normalized thermal conductance	
Structure	*x*-direction	*y*-direction
Pristine Graphene	1	1
Hex(8, 96, 24)	0.2202	0.1550
IsoTri(8, 90, 30)	0.1464	0.1007
Rect(8, 104, 28)	0.1894	0.1250

neighbor antidots of IsoTri(8,90,30). Very recently, Tan and coworkers have investigated the anisotropy of thermal conductance in graphene nanoribbons.[14] Viewing each edge in the GALs as the edge of a short ribbon, one can explain the differences between the thermal conductances. The phonon dispersion of Hex(8,96,24), which has a zigzag boundary is more dispersive, whereas IsoTri(8,90,30) has an armchair edge and as a result its phonon dispersion is less dispersive.[14] As the transmission probability is directly related to the phonon band structure, the transmission probability will be larger in Hex(8,96,24). The edges of Rect(8,104,28) are partly zigzag and armchair. Its circumference is larger than that of Hex(8,96,24), whereas it has the largest area of antidots considered. Therefore, its phonon transmission probability lies between those of Hex(8,96,24) and IsoTri(8,90,30).

The normalized thermal conductances of different GALs with respect to the thermal conductance of pristine graphene are summarized in Table I. Although the thermal conductance is anisotropic, the ratio of thermal conductances is nearly equal for the x and y-directions, which indicates the circumference and the type of the edge play a significant role in thermal conductance. Triangular GALs have the smallest thermal conductance, although they have the smallest area among the antidot shapes considered. This behavior can be explained by considering the fact that triangular antidots have the highest circumference of all antidots with the same area. In addition, they have armchair edges and, therefore, less dispersive bands. This indicates that the circumference of the antidot has a stronger effect on the thermal conductance rather than its area. The figures of merit of different GALs as a function of the Fermi energy are compared in Fig. 5. Although the maximum of the power factor of IsoTri(8,90,30) is smaller than that of Hex(8,96,24), IsoTri(8,90,30) has the highest ZT, because it has the lowest lattice thermal conductance.

Temperature Dependence

The thermoelectric power factor of GALs with different antidot shapes as a function of temperature are shown in Fig. 6-a. The

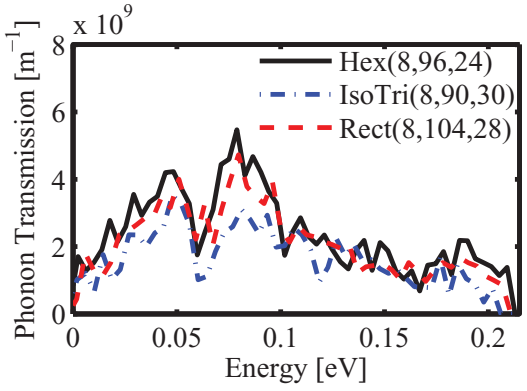

Figure 4. The phonon transmission probability of Hex(8, 96, 24), IsoTri(8, 90, 30), and Rect(8, 104, 28).

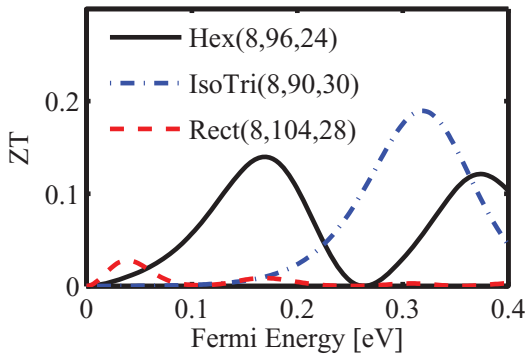

Figure 5. The figure of merit ZT of different GALs as a function of the Fermi energy.

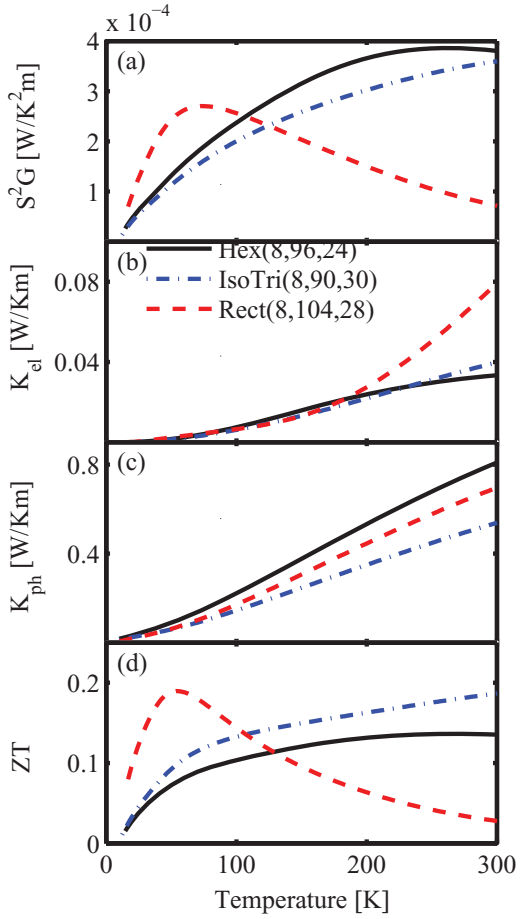

Figure 6. (a) The thermoelectric power factor, (b) the electron thermal conductance, (c) the lattice thermal conductance, and (d) the figure of merit ZT as a function of temperature.

thermal broadening function has a width of a few k_BT around E_F. Hence, at high temperature a larger band-gap is needed to improve the power factor. As a result, IsoTri(8,90,30) has the largest and Rect(8,104,28) has the smallest power factor at high temperatures. Although IsoTri(8,90,30) has the largest band-gap, Hex(8,96,24) and Rect(8,104,28) benefit from a sharp feature in the transmission at the edge of their conduction band. At temperatures below $300K$, a sharp feature in the transmission probability plays a more significant role than the band-gap. Therefore, Hex(8,96,24) has the highest power factor in the temperature range of $100K$ to $300K$. Rect(8,104,28) suffers from a narrow energy band-gap and its corresponding power factor is the smallest one at high temperature. However, its power factor increases at lower temperature and it has the highest power factor at temperatures below $100K$. In this range of temperature the width of thermal broadening is small and the sharp feature in transmission probability of Rect(8,104,28) results in a high power factor.

The temperature dependence of ZT is shown in Fig. 6-d. Although the power factor of Hex(8,96,24) is larger than that of IsoTri(8,90,30) in a wide range of temperature, its corresponding ZT is smaller than that of IsoTri(8,90,30), because of its larger lattice thermal conductance. However, the ZT of Rect(8,104,28) is the highest at low temperatures because it has a moderate lattice thermal conductance and a large power factor due to its sharp features in the transmission probability. The power factor of Rect(8,104,28) is extremely low at high temperatures because of its narrow band-gap. In addition, its corresponding electrical contribution to the thermal conductance increases significantly at high temperatures (see Fig. 6-b) due to a large factor $(E - E_F)^2$. Therefore the figure of merit of Rect(8,104,28) rapidly decreases with increasing temperature.

Conclusion

We numerically analyzed the thermoelectric properties of GALs. Our results indicate that the area and the circumference of the antidots, the type of edges, and the distance between antidots influence the thermal and thermoelectric properties of GALs. However, the circumference of the antidot plays a more important role than other geometrical parameters. In addition to the band-gap, sharp features in the transmission probability yield a high power factor, especially at extremely low temperature. We show that by appropriate selection of the geometrical parameters one can significantly reduce the thermal conductance of GALs and improve their thermoelectric figure of merit. This allows one to design and optimize the efficiency of graphene-based thermoelectric devices for future energy harvesting and other thermoelectric applications.

Acknowledgment

This work was partly supported by the Austrian Climate and Energy Fund, Contract No. 825467.

1. H. Goldsmid, *Introduction to Thermoelectricity* (Springer, 2010), chap. Review of Thermoelectric Materials.
2. L. Weber and E. Gmelin, *Appl. Phys. A*, **53**, 136 (1991).
3. A. I. Hochbaum, R. Chen, R. D. Delgado, W. Liang, E. C. Garnett, M. Najarian, A. Majumdar, and P. Yang, *Nature (London)*, **451**, 163 (2008).
4. A. Boukai, Y. Bunimovich, J. Tahir-Kheli, J.-K. Yu, W. Goddard, and J. Heath, *Nature (London)*, **451**, 168 (2008).
5. R. Venkatasubramanian, E. Siivola, T. Colpitts, and B. O'Quinn, *Nature*, **413**, 597 (2001).
6. B. Wolfing, C. Kloc, J. Teubner, and E. Bucher, *Phys. Rev. Lett.*, **86**, 4350 (2001).
7. K. Novoselov, A. Geim, S. Morozov, D. Jiang, Y. Zhang, S. Dubonos, I. Grigorieva, and A. Firsov, *Science*, **306**, 666 (2004).
8. J.-H. Chen, C. Jang, S. Xiao, M. Ishighami, and M. Fuhrer, *Nature Nanotech.*, **3**, 206 (2008).
9. D. Dragoman and M. Dragoman, *Appl. Phys. Lett.*, **91**, 203116 (3pp) (2007).
10. K. Kim, Y. Zhao, H. Jang, S. Lee, J. Kim, K. Kim, J.-H. Ahn, P. Kim, J.-Y. Choi, and B. Hong, *Nature (London)*, **457**, 706 (2009).
11. A. A. Balandin, S. Ghosh, W. Bao, I. Calizo, D. Teweldebrhan, F. Miao, and C. N. Lau, *Nano Lett.*, **8**, 902 (2008).
12. J. Hone, M. Whitney, C. Piskoti, and A. Zettl, *Phys. Rev. B*, **59**, R2514 (1999).
13. H. Sevincli and G. Cuniberti, *Phys. Rev. B*, **81**, 113401 (4pp) (2010).
14. Z. W. Tan, J.-S. Wang, and C. K. Gan, *Nano Lett.*, **11**, 214 (2011).
15. Y. Ouyang and J. Guo, *Appl. Phys. Lett.*, **94**, 263107 (3pp) (2009).
16. H. Zhang, G. Lee, A. F. Fonseca, T. L. Borders, and K. Cho, *Journal of Nanomaterials*, **2010**, 537657 (5pp) (2010).
17. J. Bai, X. Zhong, S. Jiang, Y. Huang, and X. Duan, *Nature Nanotech.*, **5**, 190 (2010).
18. T. G. Pedersen, C. Flindt, J. Pedersen, N. A. Mortensen, A.-P. Jauho, and K. Pedersen, *Phys. Rev. Lett.*, **100**, 136804 (4pp) (2008a).
19. J. Furst, J. Pedersen, C. Flindt, N. Mortensen, M. Brandbyge, T. Pedersen, and A.-P. Jauho, *New J. Phys.*, **11**, 095020 (2009).
20. T. G. Pedersen, C. Flindt, J. Pedersen, A.-P. Jauho, N. A. Mortensen, and K. Pedersen, *Phys. Rev. B*, **77**, 245431 (6pp) (2008b).
21. D. K.C. Macdonald, *Thermoelectricity: An Introduction to the Principles* (Dover Pubns, 2006).
22. J. Hone, I. Ellwood, M. Muno, A. Mizel, M. L. Cohen, and A. Zettl, *Phys. Rev. Lett.*, **80**, 1042 (1998).
23. D. Sanchez-Portal, P. Ordejon, E. Artacho, and J. M. Soler, *Int. J. Quantum Chem*, **65**, 453 (1997).
24. J. P. Perdew, K. Burke, and M. Ernzerhof, *Phys. Rev. Lett.*, **77**, 3865 (1996).
25. S. Datta, *Quantum Transport: From Atoms to Transistors* (Cambridge University Press, Cambridge, 2005).
26. T. Yamamoto, S. Watanabe, and K. Watanabe, *Phys. Rev. Lett.*, **92**, 075502 (4pp) (2004).
27. L. G.C. Rego and G. Kirczenow, *Phys. Rev. Lett.*, **81**, 232 (1998).
28. C. Jeong, R. Kim, M. Luisier, S. Datta, and M. Lundstrom, *J. Appl. Phys.*, **107**, 023707 (7pp) (2010).
29. R. Landauer, *IBM J. Res. Dev.*, **1**, 223 (9pp) (1957).
30. M. Inui, S. A. Trugman, and E. Abrahams, *Phys. Rev. B*, **49**, 3190 (1994).
31. M. Vanevic, V. M. Stojanovic, and M. Kindermann, *Phys. Rev. B*, **80**, 045410 (8pp) (2009).
32. A. Zhang, H. F. Teoh, Z. Dai, Y. P. Feng, and C. Zhang, *Appl. Phys. Lett.*, **98**, 023105 (3pp) (2011).
33. J. H. Seol, I. Jo, A. L. Moore, L. Lindsay, Z. H. Aitkenhary, M. T. Pettes, X. Li, Z. Yao, R. Huang, D. Broido, et al., *Science*, **328**, 213 (2010).
34. L. D. Hicks and M. S. Dresselhaus, *Phys. Rev. B*, **47**, 12727 (1993).